Skeletal Radiol (2000) 29:367–377

REVIEW ARTICLE

MR imaging of articular cartilage

David G. Disler
Michael P. Recht
Thomas R. McCauley

Received: 25 January 2000
Revision requested: 21 March 2000
Revision received: 31 March 2000
Accepted: 3 April 2000

D.G. Disler, M.D. (✉)
Department of Radiology,
Medical College of Virginia,
P.O. Box 980615,
Virginia Commonwealth University,
Richmond, VA 23298-0615, USA

M.P. Recht, M.D.
Division of Radiology,
Cleveland Clinic Foundation, Cleveland,
Ohio, USA

T.R. McCauley, M.D.
Department of Radiology,
Yale Medical School, New Haven,
Connecticut, USA

Abstract With the advent of new treatments for articular cartilage disorders, accurate noninvasive assessment of articular cartilage, particularly with MR imaging, has become important. Understanding the MR imaging features of articular cartilage has led to the development of two types of routinely available MR imaging techniques which have demonstrated clinical accuracy and interobserver reliability.

Key words Cartilage, MR · Joints, MR · Magnetic resonance, tissue characterization · Magnetic resonance, utilization

Introduction

MR imaging of the knee has been shown to be reliable for osseous, ligamentous and meniscal pathology [1, 2], but standard sequences that were developed for evaluation of these structures are insensitive in the detection of articular cartilage derangement [3, 4, 5, 6,7]. Prior to the evolution of surgical therapy for articular cartilage disorders, this limitation was not of substantial concern because the orthopedic surgeon could have little therapeutic impact on the dismal prognostic outcome of articular lesions to eventual osteoarthritis. However, recent advances in the treatment of articular cartilage disorders, including osteochondral autografting, autologous chondrocyte implantation, and the use of chondroprotective drugs [8, 9, 10, 11, 12, 13,14], have made it necessary to accurately predict the presence, number, and extent of articular cartilage defects. Furthermore, postoperative assessment of the integrity of cartilage grafts is now needed to determine the structural success of surgical interventions. In this review the biochemical and mechanical features of articular cartilage will be described, followed by discussion of MR imaging strategies and illustration of clinical imaging.

Articular cartilage

Articular cartilage, also called hyaline cartilage, is a glistening tissue that covers the apposing articular margins of diarthrodial joints and fulfills three requisite functions. First, it provides the means by which normal forces are transmitted with even distribution to the underlying subchondral bone [15]. Second, it permits a frictionless gliding surface for joint movement [15]. Third, it must allow the diffusion of solutes and nutrients to the cells found in articular cartilage, namely the chondrocytes [16]. Chondrocytes are highly specialized cells that produce the complex extracellular matrix responsible for the properties of articular cartilage. Articular cartilage is

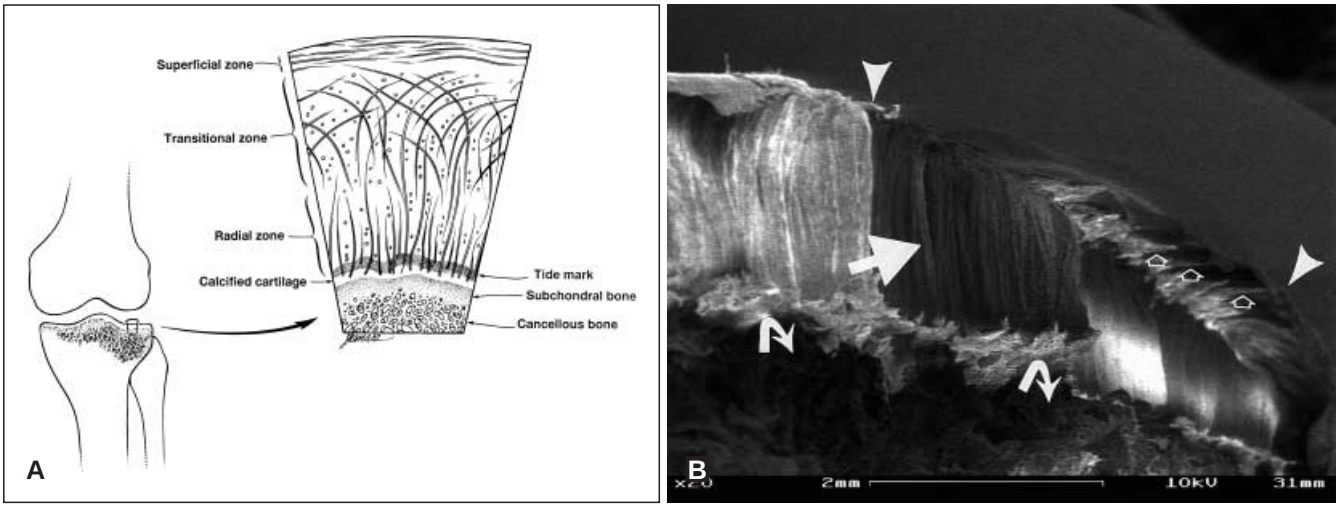

Fig. 1A,B Zonal anatomy of articular cartilage. **A** Diagram shows the zonal anatomy of articular cartilage and collagen fiber orientation. Fibers are oriented parallel to the joint surface in the superficial zone, perpendicular to the joint surface in the radial zone, and are arcade-like in their course in the transitional zone. (Adapted and reproduced, with permission, from [5].) **B** Scanning electron micrograph of proximal tibial articular cartilage shows radial (*arrow*), transitional (*open arrows*) and superficial (*arrowheads*) articular cartilage zonal orientation of collagen fibers. The lowest portion of the image is the subchondral bone (*curved arrows*). (Adapted and reproduced, with permission, from Goodwin DW, Dunn JF. High resolution magnetic resonance imaging of articular cartilage: correlation with histology and pathology. Topics Magn Reson Imaging 1998; 9:337–347)

avascular, aneural, and alymphatic, relying on solutes diffusing through the synovial fluid and, to a lesser extent, the subchondral extracellular fluid for its nutrition [16].

Articular cartilage is composed of three major extracellular constituents: water, collagen, and proteoglycan aggregates [16, 17, 18]. Water accounts for about 80% of the weight of articular cartilage, and is most abundant subjacent to the surface [18]. During surface loading, water is expressed from the matrix of cartilage and is the source of frictionless gliding that occurs during joint motion. Collagen is a triple-helical protein molecule, bundled into groups called fibrils, which in turn are bundled into fibers [15, 16]. Collagen in hyaline cartilage is primarily type II collagen [15, 16], unlike the predominant type I collagen found in tendons and ligaments. In type II collagen, there is a high concentration of terminal-amine amino acids such as lysine and hydroxylysine, which produces covalent cross-reaction between collagen molecules and fibrils and thus very stable packing that resists tensile forces [15, 17]. This tensile strength accounts for the main mechanical feature of collagen in hyaline cartilage, which is to resist shear stress [17, 18]. The anatomical distribution and orientation of collagen in articular cartilage follows these tensile lines of force [19], and allows demonstration of anatomical zones at microscopy (Fig. 1). At the surface, collagen fibers are thin, criss-crossing, and oriented parallel to the joint surface. This zone is called the superficial (tangential) zone. Deep to this zone is the transitional zone, in which fibers are oriented in sheet-like arcades with the apex of the arcade toward the joint surface. The deepest zone is the radial zone, in which are found the thickest fibers, oriented perpendicular to the joint surface. The radial zone is composed of a superficial noncalcified layer and a deeper calcified layer, separated by a histological landmark known as the tide mark. Subchondral bone is found deep to the calcified radial zone.

Proteoglycan aggregates, the third extracellular constituent of articular cartilage, are massive molecules so large that they are entrapped in the collagen framework of articular cartilage [15, 16]. These aggregates have a core chain of hyaluronic acid to which are attached a multitude of proteoglycan side units. Each proteoglycan unit is composed of a protein core to which are attached glycosaminoglycan side-chains, mostly keratan sulfate and chondroitin sulfate [15]. These chains are extremely hydrophilic due to the presence of high concentrations of sulfates, carboxylates, and hydroxyl ligands that result in anionic, osmotic, and Donnan forces within the cartilage [15, 16, 17]. The resultant enormous swelling pressure accounts for the abundance of water in articular cartilage and proteoglycan's main mechanical property, which is to resist compressive forces [15, 16, 17]. As compressive forces are exerted on the articular surface, proteoglycan and water provide mechanical resistance; the water that is expressed through the surface acts as a lubricant, diminishing friction at the surface. Proteoglycan distribution tends to follow the distribution of water content, being most abundant beneath the articular surface.

Imaging considerations

Although articular cartilage covers a large surface area in the joint, it is extremely thin. High spatial resolution techniques are therefore desirable for demonstrating articular cartilage and detecting small or shallow lesions within cartilage. In this respect, three-dimensional MR imaging techniques are favored because of the high signal-to-noise ratio that they can achieve [4, 5, 6, 7, 20, 21, 22, 23]. Furthermore, contrast resolution needs to be considered in imaging strategies because articular cartilage must be discriminated from adjacent joint fluid, bone, fat, and muscle. It is known that the T1 relaxation time of articular cartilage is approximately 1 s and is uniform [24]. T2 relaxation time in articular cartilage, however, is nonuniform and varies by depth, being approximately 35 ms in the deepest portions of articular cartilage and 70 ms superficially [24, 25, 26].

On T2-weighted conventional spin-echo MR images (Figs. 2, 3), cartilage appears as a dark structure, compared with high signal intensity fluid, intermediate signal intensity fat, and low signal intensity cortical bone. Therefore, an arthrogram-like effect is found on T2-weighted MR images when joint fluid is present [27, 28]. However, T2-weighted conventional spin-echo MR images have been found to be relatively insensitive to the detection of articular cartilage defects [4, 6, 7, 28]. On T1-weighted conventional spin-echo MR images there is insufficient contrast between cartilage, joint fluid, and fat to permit sensitive detection of articular defects [29] (Fig. 2B), unless fat suppression techniques are used to increase the dynamic range. When fat suppression is used, articular cartilage appears as a bright structure compared with adjacent tissues that are all of lower signal intensity. With the use of thin-section three-dimensional (3D) T1-weighted gradient-echo MR imaging [spoiled gradient-echo (SPGR) imaging; Fig. 2C], sufficient contrast and spatial resolution is achieved to produce images of high sensitivity and specificity to detect articular cartilage defects [4, 6, 7, 20]. Signal within articular cartilage is uniform with 3D SPGR imaging, and abnormalities most commonly appear as contour defects rather than as areas of signal change [6, 7, 20] (Fig. 4). T2* gradient-echo images are of poor sensitivity to detect articular cartilage lesions because contrast resolution between cartilage and fluid, which are both of increased signal intensity, is insufficient for lesion detection [29, 30].

Although T2-weighted conventional spin-echo images are insensitive to the detection of articular cartilage defects, intermediate-weighted and T2-weighted fast spin-echo images (Fig. 2D) have been shown to be highly sensitive, with similar results as achieved for 3D SPGR imaging [31, 32, 33, 34, 35]. This is probably due to fast spin-echo images providing magnetization transfer contrast [31], as well as T2 contrast. Magnetization transfer contrast occurs in tissues with a high concentration of macromolecules [36, 37]. Macromolecular hydrogen atoms, which are in equilibrium with hydrogen in water, exhibit a broad downfield precessional frequency range; when a presaturation pulse is delivered to this frequency, protons are saturated, resulting in lower signal on images [37]. Collagen is felt to be responsible for the magnetization transfer effect in articular cartilage [36, 38, 39]. When collagen content is diminished, as in cartilage degradation, there is decreased magnetization transfer effect, resulting in increased signal. Thus, T2-weighted fast spin-echo images show cartilage abnormalities as areas of increased signal intensity (Fig. 5).

Other means by which to perform MR imaging of articular cartilage are evolving. Diffusion-weighted MR imaging techniques may prove useful in evaluating articular cartilage because diffusion of water directly correlates with tissue hydration and has been shown to increase with cartilage degradation [40]. This concept is based on the expected lessening of the restricted motion of water in the setting of articular derangement. Furthermore, anionic contrast agents may prove useful in the evaluation of articular derangement [41, 42]. In normal articular cartilage there is a high concentration of anionic charge produced by proteoglycan aggregates. In cartilage degradation, the proteoglycan aggregates are smaller and fewer in number [17, 42], and thus the anionic charge diminishes. As expected, the distribution of anionic contrast agents inversely correlates with that of proteoglycans, and thus contrast agents concentrate in areas of articular cartilage degeneration [41, 42]. Similar enhancement in articular cartilage is seen with either intravenous or intra-articular routes of contrast administration [41].

Other techniques being investigated include using ultrashort echo times to assess the short T2 components in articular cartilage [43], using high field strength magnets to improve spatial resolution [44], and using spectroscopy and imaging generated from sodium nuclei, which are abundant in articular cartilage [45]. These techniques have all shown success in the laboratory, but have yet to be applied clinically.

Artifacts

Because MR images are acquired with high contrast and spatial resolution, certain artifacts can occur that may cause the inexperienced reader to misinterpret findings in articular cartilage on 3D SPGR and T2-weighted fast spin-echo images. The first artifact to consider is truncation artifact [46, 47]. Truncation artifact is caused by the presence of sharp borders that cannot be exactly reproduced on the image because the signal is only sampled for a finite period of time. Truncation artifact is most apparent when imaging high-contrast structures a few pixel numbers in thickness. The artifact appears as central

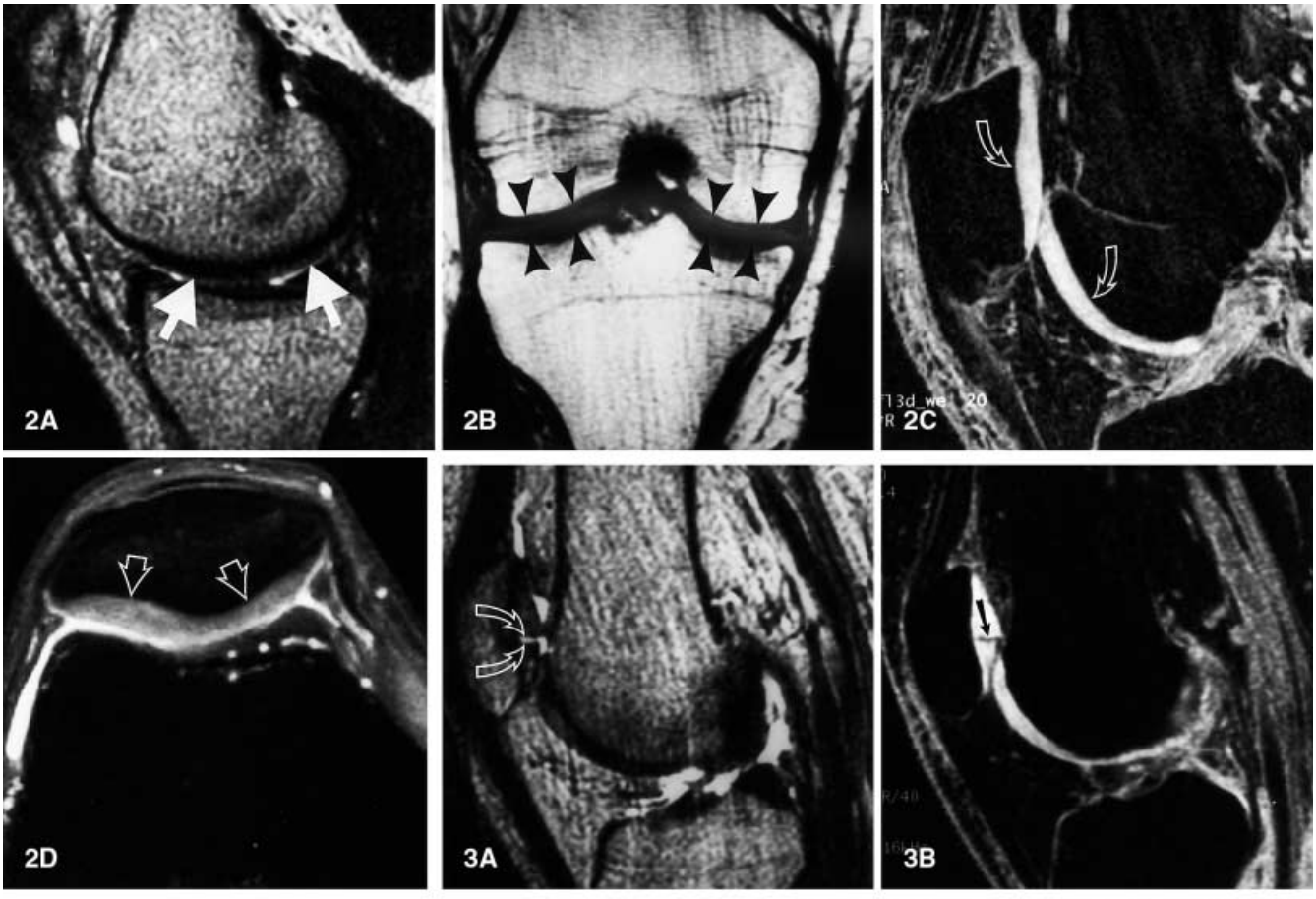

Fig. 2A–D MR images of normal hyaline cartilage. **A** Sagittal T2-weighted spin-echo image (2600/80, TR ms/TE ms) shows articular cartilage (*arrows*) as a structure of diminished signal intensity similar to fat and subchondral bone. A small amount of joint fluid provides an arthrogram-like effect due to the higher signal intensity of fluid. **B** Coronal T1-weighted spin-echo image (500/12) shows articular cartilage (*arrowheads*) as of intermediate signal intensity compared with subchondral bone, which is of diminished signal intensity, and fat, which is of high signal intensity. (Even with photographic enhancement at the level of the joint line, discrimination is difficult between the femoral and tibial articular cartilage, and between articular cartilage and subchondral bone). **C** Sagittal fat-suppressed three-dimensional spoiled gradient-echo image (32/8; flip angle, 40°) shows articular cartilage (*arrows*) as a high-signal structure compared with adjacent tissues of diminished signal intensity. **D** Axial fat-suppressed intermediate-weighted fast spin-echo image (4500/15; echo train length, 7) shows articular cartilage (*arrows*) as an intermediate-signal structure compared with the higher signal intensity of fluid and the lower signal intensity of subchondral bone

Fig. 3A,B Arthrogram-like effect on a T2-weighted image. **A** Sagittal T2-weighted spin-echo image (2600/80, TR ms/TE ms) in a patient with joint effusion shows fluid within a linear patellar articular cartilage defect (*arrows*). **B** Sagittal fat-suppressed three-dimensional spoiled gradient-echo image (32/8; flip angle, 40°) shows a linear contour defect (*arrow*) in the same area

Fig. 4 Sagittal fat-suppressed three-dimensional spoiled gradient-echo image (60/5, TR ms/TE ms; flip angle 40°) shows a large articular cartilage defect as a contour defect (*arrows*). Note that the signal in remnant articular cartilage deep to the defect is similar in signal intensity to cartilage remote from the defect. T1 of normal articular cartilage does not demonstrate spatial variation. (Adapted and reproduced, with permission, from [6])

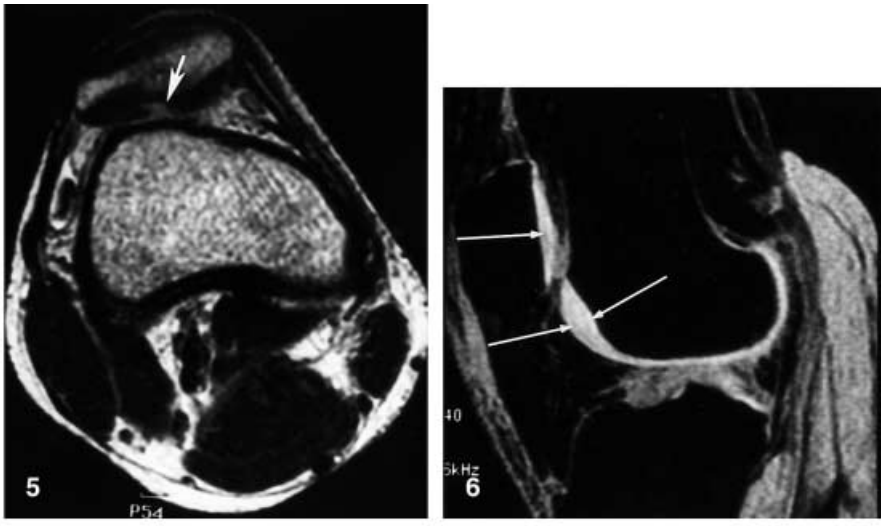

Fig. 5 Axial intermediate-weighted fast spin-echo image (4000/39, TR ms/ TE ms; echo train length, 8) shows a patellar cartilage defect (*arrow*) as a focal area of increased signal intensity

Fig. 6 Axial reformatted image of fat-suppressed three-dimensional spoiled gradient-echo MR images acquired in the sagittal plane (32/8, TR ms/TE ms; flip angle, 40°) shows truncation artifact in the patella as central linear zones of diminished signal (*arrows*) relative to the high signal of adjacent cartilage. (Adapted and reproduced, with permission, from Disler DG, McCauley TR. Clinical magnetic resonance imaging of articular cartilage. Topics Magn Reson Imaging 1998; 9:360–376)

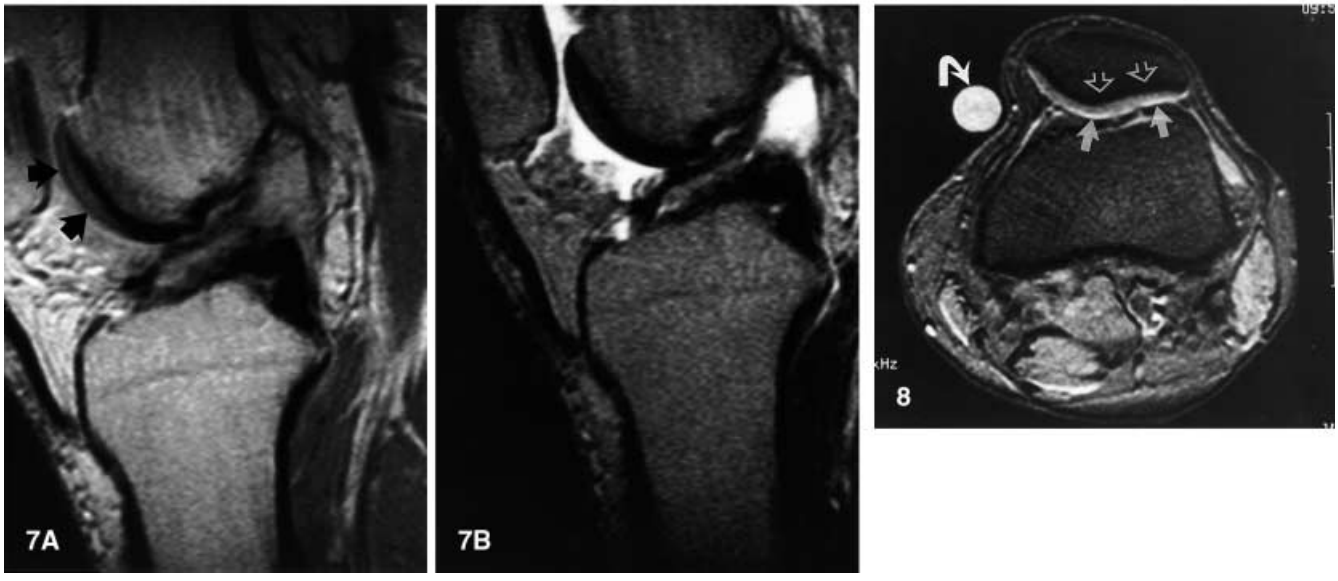

Fig. 7A,B Magic angle effect in trochlear cartilage in a 38-year-old man with an anterior cruciate ligament tear and large effusion. **A** Sagittal intermediate-weighted spin-echo image (2400/25, TR ms/TE ms) shows localized increased signal in the trochlear cartilage (*arrows*) at an angle of approximately 55° to the main magnetic field (main magnetic field craniocaudad). Compare with the reduced signal at the caudal aspect of the articular surface. **B** Sagittal T2-weighted spin-echo image (2400/90) in same patient proves the signal change in **A** is due to the magic angle effect because the signal alteration disappears with longer TE

Fig. 8 Axial gradient-echo image (450/60, TR ms/TE ms; flip angle, 20°) shows a chemical shift artifact as a band of bright signal (*arrows*) at one fat-fluid interface and a band of dark signal (*open arrows*) at the opposite fat-fluid interface. This artifact is a result of signal misregistration caused by differences in precessional frequency between hydrogen in fat and water. Frequency direction in this acquisition was anteroposterior. The round object of high signal intensity (*curved arrow*) represents a joint fluid phantom. (Adapted and reproduced, with permission, from [21])

bands of opposed signal intensity compared with the signal of the reconstructed object (Fig. 6), and the number of central bands increases with increasing number of pixels across the thickness of the object. In the case of articular cartilage, fat-suppressed 3D SPGR images display this artifact because of the high contrast achieved compared with adjacent structures [46, 47]. Truncation artifact is easily recognized and does not interfere with the detection of defects. In fact, it can be helpful in determining the depth of an articular cartilage defect [7]. Although truncation artifacts produce apparent signal lamination within articular cartilage, true laminations related to differences in T2 relaxation between anatomical cartilage layers are also seen, best demonstrated on intermediate-echo images [25, 44].

A second artifact that is commonly found in articular cartilage when using T2-weighted images is the magic angle effect [48, 49]. This artifact produces increased signal (Fig. 7) and is found in articular cartilage because

of its highly anisotropic arrangement of molecules, especially collagen [48]. Magic angle refers to the angle-dependent increase in signal intensity resulting from increased T2 in anisotropic structures that is maximal at approximately 55° relative to the main magnetic field [48, 49]. This artifact can mimic articular defects, particularly on T2-weighted images, since articular cartilage abnormalities also appear as increased signal intensity (Fig. 5). Knowledge of the expected locations of magic angle artifact can help avoid misdiagnoses; it should be expected in articular cartilage oriented at 55° to the main magnetic field, such as in the femoral trochlea. In unclear cases, attempts at re-imaging after changing the angle of the articular surface relative to the main magnetic field would be expected to cause the location of the artifact to change [49]. In addition, since the effect on T2 relaxation is small, the artifact is most apparent on short and intermediate echo-time images [48, 49]. On images obtained with longer echo times, the relative signal increase related to the artifact diminishes (Fig. 7B).

A third artifact to be aware of is chemical shift artifact, a misregistration of signal that results from hydrogen in water and fat precessing at frequencies separated by 3 ppm. This results in bands of low and high signal at fat-tissue interfaces and can be problematic in imaging cartilage at its interface with fat (Fig. 8). This effect can be minimized with the application of fat suppression. Selective water excitation provides an alternative to selective fat suppression that can substantially reduce imaging time by as much as 40% [20]. Water excitation is routinely employed at some centers for 3D SPGR imaging; however, it is not available on all MR equipment.

Clinical imaging

At our institutions, we routinely employ a combination of cartilage-sensitive MR imaging sequences to maximize the likelihood of detection of articular cartilage defects. These sequences are part of our routine protocols for knee MR imaging, and are incorporated while maintaining short overall imaging times. An example of a knee MR imaging protocol at one institution consists of coronal T1-weighted conventional spin-echo, sagittal fat-suppressed intermediate-weighted fast spin-echo, axial fat-suppressed intermediate-weighted and T2-weighted fast spin-echo, and sagittal water-excitation 3D SPGR images (with routine reformation of the SPGR images into the axial plane for patellar assessment). Total imaging time for this protocol is 18 min, and the entire examination can be completed in 30 min. While both 3D SPGR and T2-weighted fast spin-echo MR images are accurate and reliable in the detection of articular cartilage damage [4, 6, 7, 20, 32, 33, 34, 35], it has not yet been shown which technique is better. Practically speaking, they are both useful, and in our experience each has shown defects that the other sequence failed to detect (Figs. 9, 10, 11). The 3D SPGR sequence has the added benefit of superior in-plane resolution, lower slice thickness, and capability of multiplanar reformations without image distortion [50]. The fast spin-echo technique is less sensitive to metal artifact and can detect signal abnormalities in cartilage without contour defects. We feel the use of both imaging sequences enhances sensitivity of detecting articular cartilage damage compared with either technique alone. It should be noted that neither technique has shown substantial utility in the detection of early or preclinical osteoarthritis, which will likely require higher resolution techniques currently beyond the capabilities of clinical imaging [44].

The use of these protocols is important for several reasons. First, articular cartilage defects are common. One study showed that two-thirds of all patients referred for knee MR imaging who had subsequent arthroscopy were found to have defects of articular cartilage, and that one-fourth of all patients had internal derangement isolated to articular cartilage that accounted for their symptoms [7]. Second, the detection of articular defects affects the prognosis for patients who are found to have other internal derangement [51]. Finding articular defects is therefore important to an orthopedic surgeon advising a patient of the likelihood of clinical improvement after surgery for meniscal tears in the setting of superimposed cartilage abnormality.

Articular injury

The response to injury in articular cartilage is highly dependent on whether the injury extends to the subchondral bone plate [16, 52]. Articular cartilage cannot regenerate [17]. Once an articular defect occurs, there is an irreversible trend toward worsening of the overall articular status due to alteration in biomechanical strain in articular cartilage, with extension of the abnormality. If an articular cartilage defect extends to bone (osteochondral or transchondral injury), then a repair response occurs with development of a blood clot, release of growth factors, migration of undifferentiated mesenchyme, and the development of a partial fibrous repair consisting primarily of type I collagen [52]. The repair typically is insufficient to restore normal biomechanical status to the articular surface, and the repair material breaks down and osteoarthritis eventually ensues [52].

Chondral defects that result from injury are typically large and sharply marginated (Fig. 12). They result from shear forces and can therefore occur at the surface, or deep to the surface. Injuries in the deeper layers of hyaline cartilage are seen clinically as flap tears (Fig. 13) or chondromalacia (subsurface defect that is not apparent visually at arthroscopy but detected as softness to probing). Hyaline cartilage may be found deep to the defect if

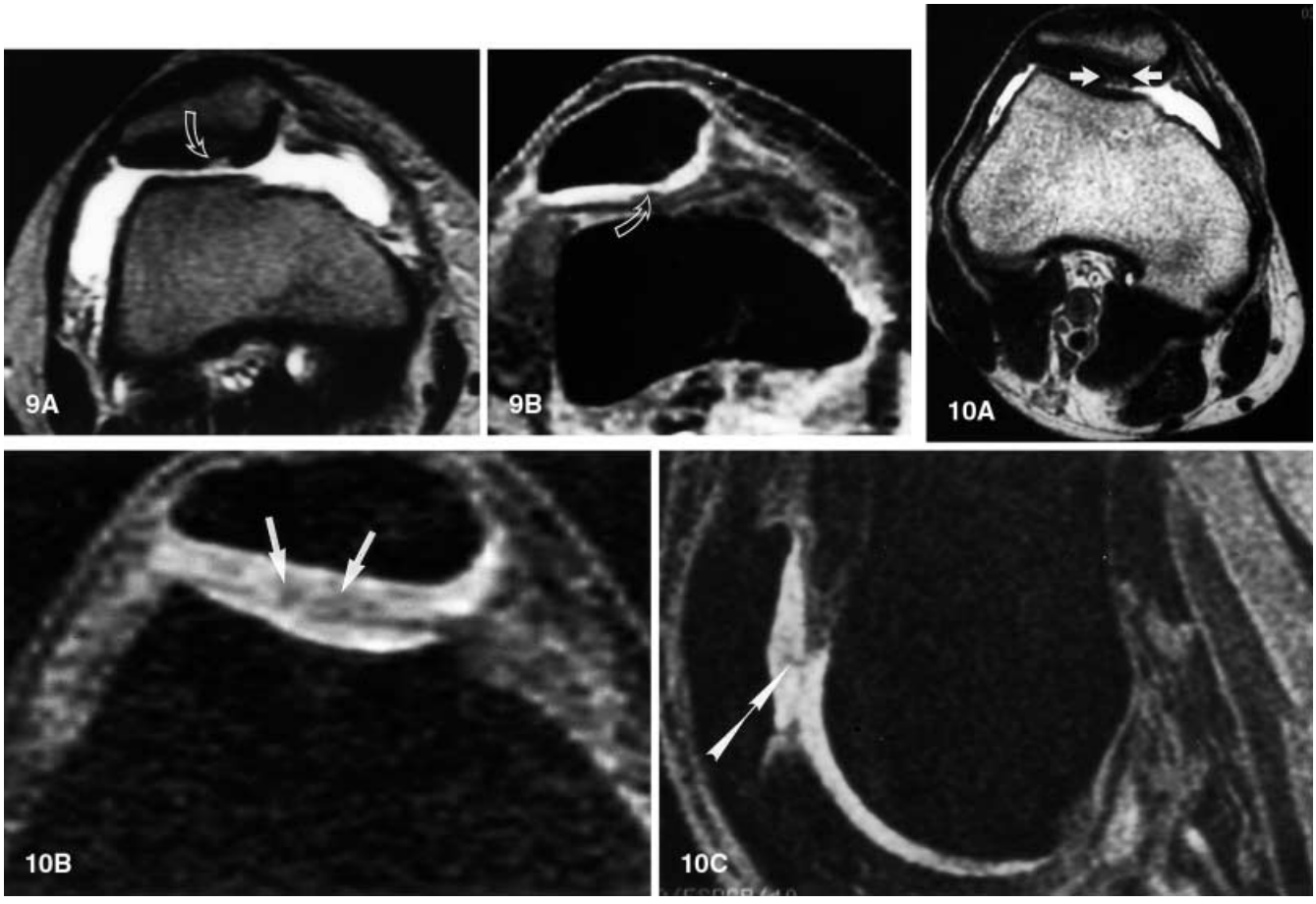

Fig. 9A,B Articular derangement that is equally apparent on intermediate-weighted fast spin-echo and spoiled gradient-echo images. **A** Axial T2-weighted fast spin-echo image (4000/91, TR ms/TE ms) demonstrates localized increased signal (*arrow*) along the lateral patellar facet. **B** Axial reformatted image of fat-suppressed three-dimensional spoiled gradient-echo MR images acquired in the sagittal plane (32/8; flip angle, 40°) shows a contour defect (*arrow*) at the lateral patellar facet

Fig. 10A–C Articular derangement better shown on a fast spin-echo image compared with a spoiled gradient-echo image. (Adapted and reproduced, with permission, from Disler DG, McCauley TR. Clinical magnetic resonance imaging of articular cartilage. Topics Magn Reson Imaging 1998; 9:360–376.) **A** Axial intermediate-weighted fast spin-echo image (4000/39, TR ms/TE ms; echo train length, 8) shows a localized area of increased signal (*arrows*) in the lateral patellar facet. **B** Axial reformatted image of fat-suppressed three-dimensional spoiled gradient-echo MR images acquired in the sagittal plane (32/8; flip angle, 40°) barely demonstrates the abnormality (*arrows*). **C** Sagittal fat-suppressed three-dimensional spoiled gradient-echo image (32/8; flip angle, 40°) shows the defect slightly better (*arrow*)

the defect is incomplete, but more typically the defects are full-thickness or nearly full-thickness defects, often with underlying bone signal changes. Subtle changes in subchondral bone signal intensity are useful clues to the presence of an overlying articular cartilage injury. In the more obvious occurrence of subchondral fracture lines (osteochondral injury), accurate assessment of the overlying articular cartilage becomes important because this assessment will determine the patient's subsequent clinical care. A stable osteochondral injury indicates that the articular cartilage overlying an osteochondral injury is intact, whereas an unstable injury indicates the articular cartilage overlying an osteochondral injury is not intact and risks displacement. Stable osteochondral injuries are treated conservatively, while unstable injuries are treated with surgical fixation or debridement. Optimal imaging of articular cartilage with MR imaging helps differentiate unstable lesions from stable ones [53].

Osteoarthritis

The appearance of osteoarthritis at MR imaging differs substantially from chondral and osteochondral injury. While the causes of osteoarthritis may be multifactorial, the evolution of pathological changes is uniform [16, 17, 52]. Intrinsic and extrinsic repair waxes and wanes [52] and is evident on MR imaging. Intrinsic repair refers to chondrocyte hyperplasia and production of extracellular matrix, whereas extrinsic repair refers to changes in ad-

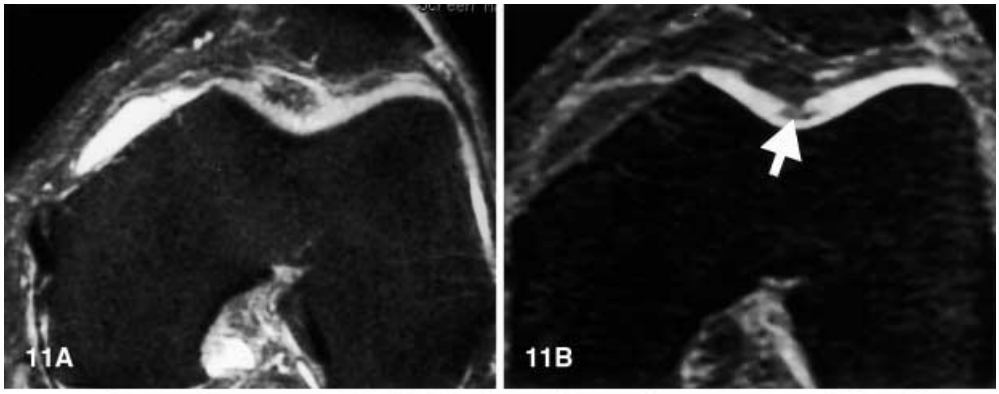

Fig. 11A–D Articular derangement shown on a spoiled gradient-echo image but not apparent on a fast spin-echo image. **A** Axial intermediate-weighted fast spin-echo image (4000/20, TR ms/TE ms; echo train length, 10) appears normal. **B** Axial reformatted image of fat-suppressed three-dimensional spoiled gradient-echo MR images acquired in the sagittal plane (40/6; flip angle, 40°) shows the defect (*arrow*). **C** Photographic image obtained during arthroscopy shows the trochlear defect (*arrows*). **D** Photographic image obtained during arthroscopy shows a metal probe (*arrow*) inserted into the defect (*arrowheads*)

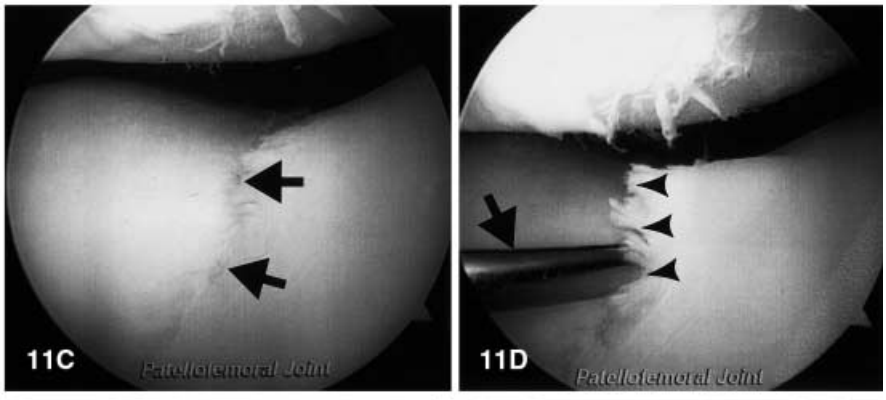

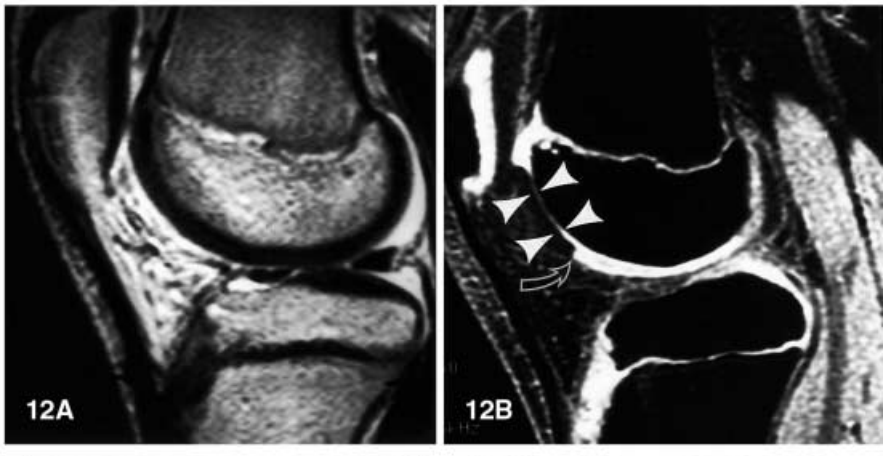

Fig. 12A,B Acute chondral defect in a 14-year-old soccer player. (Adapted and reproduced, with permission, from [6].) **A** Sagittal T2-weighted spin-echo image (1700/80, TR ms/TE ms) shows no abnormality in the femoral trochlea. **B** Sagittal fat-suppressed three-dimensional spoiled gradient-echo image (60/5; flip angle, 40°) a shows large full-thickness defect (*arrowheads*). Note the abrupt margins of the defect (*open arrow*). A cartilaginous loose body was present in the suprapatellar recess (not shown)

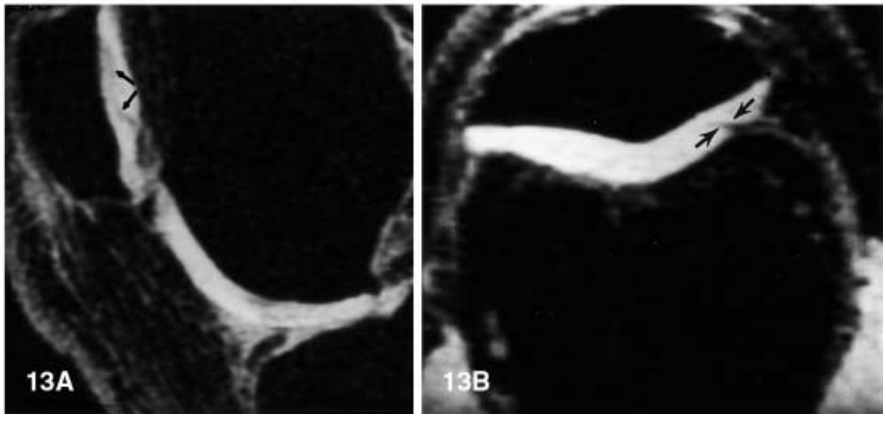

Fig. 13A,B Sagittal fat-suppressed three-dimensional spoiled gradient-echo image (32/8, TR ms/TE ms; flip angle, 40°) **(A)** and axial reformation **(B)** shows a flap tear (*arrows*) of the medial patellar facet articular cartilage

Fig. 14 Sagittal fat-suppressed three-dimensional spoiled gradient-echo image (46/6, TR ms/TE ms; flip angle, 40°) demonstrates the typical features of osteoarthritis, with multiple articular cartilage defects (*arrows*) at opposing weight-bearing margins of the lateral compartment of the knee. Note that the defect margins are obtusely angled (*arrowheads*). Compare with the abrupt margins of the acute cartilage defect in Fig. 12B. (Adapted and reproduced, with permission, from Disler DG, McCauley TR. Clinical magnetic resonance imaging of articular cartilage. Topics Magn Reson Imaging 1998; 9:360–376)

Fig. 15A,B One-year follow-up MR imaging evaluation of a patient who had undergone an autologous osteochondral transplant to a cartilage defect site at the weight-bearing surface of the lateral femoral condyle. **A** Sagittal intermediate-weighted fast spin-echo image (3833/30, TR ms/TE ms; echo train length, 12) shows the transplant site with cartilage-like signal (*arrows*). The osseous portion of graft is no longer apparent as it has incorporated into adjacent bone. **B** Sagittal fat-suppressed three-dimensional spoiled gradient-echo image (40/6; flip angle, 40°) shows overlying cartilage-like signal at the transplant site (*arrows*). There is no metallic artifact interfering with visualization of the articular cartilage. Note the osteophytes at the margin of the graft and the mildly incongruous articular surface

jacent tissues such as osteophyte formation, subchondral sclerosis, and synovial hypertrophy with hyaluronan production in synovial fluid [52]. On MR images, cartilage defects due to osteoarthritis are distinguished from the defects of chondral injury. First, in osteoarthritis there are usually multiple defects or diffuse cartilage thinning. Second, the defects are variable in size and depth. Third, the margins of defects in osteoarthritis are typically broadly obtuse in angulation (Fig. 14), whereas chondral defects from injury are acutely marginated. Finally, MR images of patients with osteoarthritis show features of extrinsic repair such as osteophyte formation and subchondral sclerosis.

Postoperative imaging

The area of postoperative imaging has not been formally explored in the literature, though there are studies in progress at several institutions evaluating the usefulness of MR imaging for assessment of autologous osteochondral transplantation or chondrocyte implantation. Fat-suppressed 3D SPGR images have a theoretical disadvantage relative to fast spin-echo images in that gradient-echo images are more prone to susceptibility artifact from retained microscopic metal, although this artifact is often not manifested on the MR images (Fig. 15). Small areas of metallic artifact can be seen at chondral surgery sites and can interfere with evaluation for neocartilage thickness and surface smoothness. The signal in new cartilage is similar to that of adjacent native cartilage, but histological and biomechanical correlations of neocartilage versus native cartilage have not been rigorously studied. The ultimate advantage of MR imaging over invasive means of postoperative cartilage assessment will lie in the lower cost, increased patient acceptance, and increased opportunities for more frequent assessment than is now possible with postoperative arthroscopy. The ultimate efficacy of MR imaging, however, awaits assessment with a large cohort of patients with correlation with surgical findings and tests of observer performance.

Summary

MR imaging of articular cartilage can be rapidly performed and incorporated into routine protocols without substantial increase in imaging times. There are many practical reasons to image articular cartilage, and two clinically useful MR imaging sequences include fat-suppressed 3D SPGR and T2-weighted fast spin-echo imaging. Both have been shown to be accurate and reliable in the detection of articular cartilage derangement. MR imaging of articular cartilage will continue to grow in importance with acceptance of the technique in predicting prognosis of cartilage lesions and identifying candidates for cartilage treatment.

References

1. Mink JH, Levy T, Crues JV. Tears of the anterior cruciate liagment and menisci of the knee: MR imaging evaluation. Radiology 1988; 167:769–774.
2. Mink JH, Deutsch AL. Occult cartilage and bone injuries of the knee: detection, classification, and assessment with MR imaging. Radiology 1989; 170:823–829.
3. Gagliardi JA, Chung EM, Chandnani VP, et al. Detection and staging of chondromalacia patellae: relative efficacies of conventional MR imaging, MR arthrography, and CT arthrography. AJR 1994; 163:629–636.
4. Recht MP, Kramer J, Marcelis S, et al. Abnormalities of articular cartilage in the knee: analysis of available MR techniques. Radiology 1993; 187:473–478.
5. Recht MP, Resnick D. MR imaging of articular cartilage: current status and future directions. AJR 1994; 163:283–290.
6. Disler DG, McCauley TR, Wirth CR, Fuchs MD. Detection of knee hyaline cartilage defects using fat-suppressed three-dimensional spoiled gradient-echo MR imaging: comparison with standard MR imaging and correlation with arthroscopy. AJR 1995; 165:377–382.
7. Disler DG, McCauley TR, Kelman CG, et al. Fat-suppressed three-dimensional spoiled gradient-echo MR imaging of hyaline cartilage defects in the knee: comparison with standard MR imaging and arthroscopy. AJR 1996; 167:127–132.
8. Laszlo H, Kish G, Karpati Z, Eberhardt R. Osteochondral plugs: autogenous osteochondral masaicplasty for the treatment of focal chondral and osteochondral articular defects. Operative Techniques Orthop 1997; 7:312–322.
9. Brittberg M, Lindahl A, Nilsson A, Ohlsson C, Isaksson O, Peterson L. Treatment of deep cartilage defects in the knee with autologous chondrocyte transplantation. N Engl J Med 1994; 331:889–895.
10. Chen FS, Frenkel SR, DiCesare PE. Chondrocyte transplantation and experimental treatment options for articular cartilage defects. Am J Orthop 1997; 26:396–406.
11. Hangody L, Karpati Z, Sukosd L. Autogenous osteochondral mosaic technique. Rev Osteol 1996; 3:70–73.
12. Mankin HJ, Buckwater JA. Restoration of the osteoarthritic joint. J Bone Joint Surg Am 1996; 78:1–2.
13. Ghosh P, Wells C, Smith M, Hutadiolok N. Chondroprotection, myth or reality: an experimental approach. Semin Arthritis Rheum 1990; 19:3–9.
14. Howell DS, Altman RD. Cartilage repair and conservation in osteoarthritis. Rheum Dis Clin North Am 1993; 19:713–724.
15. Akeson WH, Amiel DA, Gershuni DH. Articular cartilage physiology and metabolism. In: Resnick D, ed. Diagnosis of bone and joint disorders, 3rd edn. Philadelphia: WB Saunders, 1995: 769–790.
16. Buckwalter JA, Mankin HJ. Articular cartilage. I. Tissue design and chondrocyte matrix interactions J Bone Joint Surg Am 1997; 79:600–611.
17. Buckwalter JA, Mow VC. Cartilage repair in osteoarthritis. In: Moskowitz RW, Howell DS, Goldberg VM, Mankin HJ, eds. Osteoarthritis, 2nd edn. Philadelphia: WB Saunders, 1992: 71–107.
18. Mankin HJ, Brandt KD. Biochemistry and metabolism of articular cartilage in osteoarthritis. In: Moskowitz RW, Howell DS, Goldberg VM, Mankin HJ, eds. Osteoarthritis, 2nd edn. Philadelphia: WB Saunders, 1992; 109–154.
19. Benninghoff A. Form und Bau der Gelenkknorpel in ihren Beziehungen zur Funktion. Anat Entwicklungsgesch 1925; 76:43.
20. Recht MP, Piraino DW, Paletta GA, Schils JP, Belhobek GH. Accuracy of fat-suppressed three-dimensional spoiled gradient-echo FLASH MR imaging in the detection of patellofemoral articular cartilage abnormalities. Radiology 1996; 198:209–212.
21. Disler DG, Peters TL, Muscoreil SJ, et al. Fat-suppressed spoiled GRASS imaging of knee hyaline cartilage: technique optimization and comparison with conventional MR imaging. AJR 1994; 163:887–892.
22. Reiser MF, Bongartz G, Erlemann R, et al. Magnetic resonance in cartilaginous lesions of the knee joint with three-dimensional gradient-echo imaging. Skeletal Radiol 1988; 17:465–471.
23. Heron CW, Calvert PT. Three-dimensional gradient-echo MR imaging of the knee: comparison with arthroscopy in 100 patients. Radiology 1992; 183:839–844.
24. Dardzinski BJ, Mosher TJ, Li S, Van Slyke MA, Smith MB. Spatial variation of T2 in human articular cartilage. Radiology 1997; 205:546–550.
25. Rubenstein JD, Kim JK, Henkelman RM. Effects of compression and recovery on bovine articular cartilage: appearance on MR images. Radiology 1996; 201:843–850.
26. Mlynarik V, Degrassi A, Toffanin R, Vittur F, Cova M, Pozzi MR. Investigation of laminar appearance of articular cartilage by means of magnetic resonance microscopy. Magn Reson Imaging 1996; 14:435–442.
27. McCauley TR, Kier R, Lynch KJ, Jok P. Chondromalacia patellae: diagnosis with MR imaging. AJR 1992; 158:101–105.
28. Yulish BS, Montanez J, Goodfellow DB, Bryan PJ, Mulopulos GP, Modic MT. Chondromalacia patellae: assessment with MR imaging. Radiology 1987; 164:763–766.
29. Hodler J, Berthiaume MJ, Schweitzer NM, Resnick D. Knee joint hyaline cartilage defects: a comparative study of MR and anatomic sections. J Comput Assist Tomogr 1992; 16:597–603.
30. Speer KP, Spritzer CE, Goldner JL, Garrett WE. Magnetic resonance imaging of traumatic knee articular cartilage injuries. Am J Sports Med 1991; 19:396–402.
31. Yao L, Gentili A, Thomas A. Incidental magnetization transfer contrast in fast spin-echo imaging of cartilage. J Magn Reson Imaging 1996; 6:180–184.
32. Potter HG, Linklater JM, Allen AA, Hannafin JA, Haas SB. Magnetic resonance imaging of articular cartilage in the knee: an evaluation with use of fast-spin-echo imaging. J Bone Joint Surg Am 1998; 80:1276–1284.
33. Sonin AH, Roychowdhury S, Fonner BT, Fitzgerald SW. Grading the articular cartlage of the patellofemoral joint with a double-echo spin-echo sequence pair [abstract]. Fifth scientific meeting of the International Society of Magnetic Resonance in Medicine, 1997:34.
34. Broderick LS, Turner DA, Renfrew DL, Schnitzer TJ, Huff JP, Harris C. Severity of articular cartilage abnormality in patients with osteoarthritis: evaluation with fast spin-echo MR vs arthroscopy. AJR 1994; 162:99–103.
35. Bredella MA, Tirman PFJ, Peterfy CG, Zarlingo M, Feller JF, Bost FW, Belzer JP, Wischer TK, Genant HK. Accuracy of T2-weighted fast spin-echo MR imaging with fat saturation in detecting cartilage defects in the knee: comparison with arthroscopy in 130 patients. AJR 1999; 172:1073–1080.
36. Gray ML, Burstein D, Lesperance LM, Gehrke L. Magnetization transfer in cartilage and its constituent macromolecules. Magn Reson Med 1995; 34:319–325.

37. Wolff SD, Chesnick S, Frank JA, Lim KO, Balaban RS. Magnetization transfer contrast: MR imaging of the knee. Radiology 1991; 179:623–628.
38. Seo GSS, Aoki J, Moriya H, et al. Hyaline cartilage: in vivo and in vitro assessment with magnetization transfer imaging. Radiology 1996; 201:525–530.
39. Kim DK, Ceckler TL, Hascall VC, Calabro A, Balaban RS. Analysis of water-macromolecule proton magnetization transfer in articular cartilage. Magn Reson Med 1993; 29:211–215.
40. Burstein D, Gray ML, Hartman AL, Gipe R, Foy BD. Diffusion of small solutes in cartilage as measured by nuclear magnetic resonance (NMR) spectroscopy and imaging. J Orthop Res 1993; 11:465–478.
41. Bashir A, Gray ML, Boutin RD, Burstein D. Glycosaminoglycan in articular cartilage: in vivo assessment with delayed Gd-$(DTPA)^{2-}$-enhanced MR imaging. Radiology 1997; 205:551–558.
42. Bashir A, Gray M, Boutin RD, Burstein D. $Gd(DTPA)^{2-}$ as a measure of cartilage degradation. Magn Reson Med 1996; 36:665–673.
43. Brossmann J, Frank LR, Pauly JM, et al. Short echo time projection reconstruction MR imaging of cartilage: comparison with fat-suppressed spoiled GRASS and magnetization transfer contrast MR imaging. Radiology 1997; 203:501–507.
44. Rubenstein JD, Li JG, Majumdar S, Henkelman RM. Image resolution and signal-to-noise ratio requirements for MR imaging of degenerative cartilage. AJR 1997; 169:1089–1096.
45. Insko EK, Reddy R, Leigh JS. High resolution, short echo time sodium imaging of articular cartilage. J Magn Reson Imaging 1997; 7:1056–1059.
46. Frank LR, Brossmann J, Buxton RB, Resnick D. MR imaging truncation artifacts can create a false laminar appearance in cartilage. AJR 1997; 168:547–554.
47. Erickson SJ, Waldschmidt JG, Czervionke LF, Prost RW. Hyaline cartilage: truncation artifact as a cause of trilaminar appearance with fat-suppressed three-dimensional spoiled gradient-recalled sequences. Radiology 1996; 201:260–264.
48. Erickson SJ, Prost RW, Timins ME. The "magic angle" effect: backround physics and clinical relevance. Radiology 1993; 188:23–25.
49. Rubenstein JD, Kim JK, Morava-Protzner I, Stanchev PL, Henkelman RM. Effects of collagen orientation on MR imaging characteristics of bovine articular cartilage. Radiology 1993; 188:219–226.
50. Piplani MA, Disler DG, McCauley TR, Holmes TJ, Cousins JP. Articular cartilage volume in the knee: semiautomated determination from three-dimensional reformations of MR images. Radiology 1996; 198:855–859.
51. Northmore-Ball MD, Dandy DJ, Jackson RW. Arthroscopic, open partial, and total meniscectomy: a comparative study. J Bone Joint Surg Br 1983; 65:400–404.
52. Buckwalter JA, Mankin HJ. Articular cartilage. II. Degeneration and osteoarthrosis, repair, regeneration, and transplantation. J Bone Joint Surg Am 1997; 79:612–632.
53. De Smet AA, Fisher DR, Graf BK, Lange RH. Osteochondritis dissecans of the knee: value of MR imaging in determining lesion stability and the presence of articular cartilage defects. AJR 1990; 155:549–553.